# Microscopic Studies of Calcium Sulfate Crystallization and Transformation at Aqueous-Organic Interfaces

*Emma R. Ravenhill,[1] Paul M. Kirkman,[2] and Patrick R. Unwin*[*1]*

1 Department of Chemistry, University of Warwick, Gibbet Hill Rd, Coventry, CV4 7AL, UK.

2 Lubrizol Ltd., The Knowle, Nether Lane, Hazelwood, Derby, DE56 4AN, UK.

[*] To whom correspondence should be addressed: P.R.Unwin@warwick.ac.uk

**Abstract**

The calcium sulfate crystal system is of considerable fundamental and practical interest, consisting of the three hydrates, gypsum ($CaSO_4 \cdot 2H_2O$), bassanite ($CaSO_4 \cdot 0.5H_2O$) and anhydrite ($CaSO_4$). Each have significant applications, however, synthesis of anhydrite via conventional aqueous methods requires elevated temperatures and therefore high energy costs. Herein, we investigate calcium sulfate crystal growth across a non-miscible aqueous-organic (hexane or dodecane) interface. This process is visualized via in situ optical microscopy, which produces high magnification videos of the crystal growth process. The use of interferometry, Raman spectroscopy and X-ray diffraction allows the full range of calcium sulfate morphologies and hydrates to be analyzed subsequently in considerable detail. In the case of dodecane, gypsum is the final product, but the use of hexane in an open (evaporating) system results in anhydrite crystals, via gypsum, at room temperature. A dissolution-precipitation mechanism between neighboring microcrystals is responsible for this transformation. This work opens up a simple new crystal synthesis route for controlling and directing crystallization and transformation.

## Introduction

Control over polymorphism is currently a key motivation in crystal research, whereby conditions are sought to selectively synthesize specific crystalline materials. The discovery of simple, low-energy pathways for the growth of highly desirable and unstable polymorphs with vital industrial and biological applications is particularly important.[1-10]

Numerous examples of high level control over polymorphism have been established for both organic[1-3] and inorganic[4-8] crystal systems. In particular, the calcium carbonate crystal system has been extensively studied.[4-7,9,10] Crystal growth additives such as natural protein-mimics[4,10] and polymers[5-7] are commonly used to achieve the growth of the metastable polymorphs, vaterite and aragonite, at much lower temperatures than otherwise possible.

Recent work demonstrates that full control is also achievable for calcium sulfate,[8,11] a system that has been explored to a much lesser extent. The calcium sulfate system consists of three intriguing crystal structures, with different degrees of hydration. Hydrates are crystalline solids containing molecular water within the crystal structure, and are named based on the number of water molecules per parent molecule (e.g. hemihydrate, dihydrate).[12-14] The most thermodynamically stable phase of calcium sulfate at room temperature is the dihydrate, gypsum ($CaSO_4 \cdot 2H_2O$) and, as a consequence, it is highly abundant in nature.[11,15-22] Both the hemihydrate, bassanite ($CaSO_4 \cdot 0.5H_2O$) and the anhydrous form, anhydrite ($CaSO_4$) are relatively thermodynamically unstable and kinetically unfavorable under ambient conditions, but each has important industrial applications. Bassanite (more commonly known as plaster of Paris), is a highly valuable building material, whereas anhydrite has applications as a binder in cements and adhesives.[8] Thus, understanding and controlling the growth of these unstable hydrates under ambient conditions is of great interest.

Although gypsum is the most thermodynamically stable hydrate at room temperature, anhydrite is more stable at elevated temperatures.[15,18,20-25] There is much debate as to the transition temperature. Previous reported values under atmospheric conditions generally fall within the broad range of 42 – 60 °C,[15,26] although in practice, it is extremely difficult to synthesize anhydrite at temperatures lower than 70 °C.[18,25,27] Anhydrite has a much higher surface free energy than gypsum (0.090 J $m^{-2}$ and 0.040 J $m^{-2}$ for anhydrite and gypsum, respectively, at 80 °C in solutions containing 0.8 M NaCl and 0.1 M $H_2SO_4$),[25] and given the third power dependence of nucleation rate on surface free energy, anhydrite grows at an extremely slow rate compared to gypsum.[27-29] Anhydrite growth is thus rarely realized even at temperatures where it is the most thermodynamically stable form of calcium sulfate. This is another reason why it is difficult to assign a precise value for the transition temperature.

Several methods have been investigated to reduce the gypsum-anhydrite transition temperature. Decreasing the water activity of the crystal growth solution has been shown to be effective, and this can be achieved by employing salts such as sodium chloride.[15,18,25-27] Crystal growth inhibitors have also been shown to favor the formation of anhydrite.[17] Finally, anhydrite seeding is often employed to bias growth towards the metastable hydrates.[18,26] However, for all of these methods, anhydrite growth has still not been accomplished at ambient temperatures, and even at the elevated temperatures employed, it often took days or even weeks for conversion to be realized.

Although there has been little success in establishing moderate conditions for the synthesis of dehydrated calcium sulfate hydrates in aqueous systems, recent work reveals that, through the use of organic solvents, it is possible to precipitate phase-pure bassanite and anhydrite nanoparticles at room temperature, as a consequence of greatly decreasing and controlling the water content of the solvent.[8,11] More broadly, there are several examples where organic solvents

have been exploited to study both the mechanisms and kinetics of crystallization, as well as crystal morphology.[30,31]

In this paper, a two-phase, non-miscible, liquid-liquid (water-hexane or water-dodecane) system was employed, with the aqueous phase providing a source of $SO_4^{2-}$ and the organic phase containing a $Ca^{2+}$ source. Comparison of dodecane and highly volatile hexane as organic solvents in an open system permitted investigation of the effect of solvent evaporation on calcium sulfate crystallization and transformation. In situ optical microscopy analysis of the aqueous-organic interfacial region during the crystal growth process allowed elucidation of the crystal morphologies and hydrates formed. New perspectives on the formation of anhydrite, which does not readily grow at room temperature, are revealed. Our studies reinforce other work that show oil-water interfaces may be used to effectively promote the growth of crystals.[32] To the best of our knowledge, this is the first time the gypsum-anhydrite phase transformation has been observed and microscopically analyzed at room temperature, and opens up new ideas and methodology for the formation of unstable hydrates under low-energy conditions.

## Experimental Section

### Crystal Growth Experiments

All aqueous solutions contained 0.5 M $H_2SO_4$ (Fischer Scientific, $\geq$ 95%) as a sulfate source and were prepared using ultrapure water (Milli-Q Reagent, Millipore) with a typical resistivity of 18.2 MΩ cm at 25 °C. Two organic solvents (VWR) were studied separately: n-hexane and n-dodecane, which have fast and negligible evaporation rates, respectively. In these, 2 wt % of an oil-soluble overbased detergent (donated by Lubrizol) was dissolved. This contained a 10 nm 400 total base number (TBN) amorphous calcium carbonate core (0.35 M),

surrounded by long-chain alkyl-sulfonate groups, ensuring the calcium source was fully dispersed within the organic phase.

Calcium sulfate crystallization and transformation was investigated by monitoring crystal growth across an aqueous-organic interface, assembled on 47 mm diameter circular glass slides (Thermo Scientific) that were cleaned thoroughly with ultrapure water, ethanol (VWR, ≥ 99.9%), and blown dry using nitrogen gas (BOC). These were fitted into Petri dishes (Willco Wells) equipped with a perspex rim and lid. In each experiment, 2 mL of the organic phase was added and a small aqueous droplet (either 1 or 20 μL) was pipetted underneath, directly onto the glass slide at the center of the Petri dish.

**Analysis of Crystal Morphologies**

A Leica DM4000 M optical microscope was used to monitor crystal growth in situ. A range of magnifications were used, depending on the sample area analyzed. Crystal growth of the entire interface of a 1 μL droplet was imaged using a 2.5× objective lens, whereas greater magnifications and larger droplets (20 μL) were used to image crystal growth at higher resolution, at a section of the aqueous-organic interface (20×) and within the bulk oil (100×). A series of time-lapse images were taken throughout the crystal growth process to provide information on the dynamic processes occurring in each of these areas. At the end of the crystal growth process, interferometry was used to analyze the topography of selected crystals using a Contour GT-I 3D Optical Microscope. Images were obtained using a 50× objective lens and processed using SPIP (6.0.14, Image Metrology) software.

**Analysis of Crystal Hydrates**

Crystals selected for interferometry were further analyzed using Raman spectroscopy to determine the hydrate. Spectra were obtained using a Renishaw micro-Raman inVia spectrometer. Regions of interest were selected using an optical microscope with a 50× objective lens. The 633 nm line of a HeNe laser was used at 100 % power, with an acquisition time of 30 s for each spectrum. Due to the small laser spot size (515 nm radius), it was possible to resolve and obtain spectra for individual crystals. Spectral calibration was performed using the 520.7 nm peak of a silicon standard, and reference spectra were obtained for natural gypsum (St. Gobain Gyproc), bassanite (formed by heating natural gypsum, cleaved along the [010] plane, dehydrated at 200 °C using a Mettler Toledo DSC1-Star instrument under an inert $N_2$ atmosphere) and natural anhydrite (UKGE Limited).

Powder X-ray diffraction (XRD) provided further information on the crystals present in each sample. A PANalytical X'Pert Pro X-Ray MPD Powder Diffractometer equipped with a curved Ge Johnasson monochromator was used, giving focused Cu $K_{\alpha 1}$ radiation (1.540598 Å), with a Pixcel detector. Scans were obtained ranging from 5 to 60° in 2θ. Crystalline structures were identified using reference patterns from the HighScore Plus software (PANalytical B. V.) and the latest ICDD powder diffraction database.

**Karl Fischer Water Content Tests**

The water contents of pure hexane and dodecane solvents, as well as bulk solutions of hexane and dodecane containing 0.35 M $CaCO_3$ overbased detergent particles were determined by Karl Fischer volumetric titration, using a Mettler DL 35 titrimeter fitted with a DM 143-SC electrode. Sample masses were determined using a Precisa EP220A balance and Aqualine Titrant 5 (Fischer) was used as a titrant. A reference standard of Analar Distilled Water (ReAgent) was

used. All samples tested contained less than 0.5 wt % water, which corresponds to an internal repeatability value quoted for this setup of ± 0.02 wt %.

**Solvent Evaporation Rates**

The evaporation rates of hexane and dodecane were measured by filling the same Petri dishes used for crystal growth experiments with 2 mL of solvent and recording the weight of solvent remaining at minute intervals over a 1 hour period. This procedure was carried out twice for each solvent, and results were averaged to give the percentage solvent weight remaining as a function of time.

**Results and Discussion**

**Crystal Growth Characteristics in the Aqueous-Dodecane System**

The experimental setup used to microscopically monitor crystal growth is shown in Figure 1. Images were acquired from above the sample, providing a view of the whole circumference of the aqueous-organic interface when small aqueous droplets (1 μL volume) and low magnifications (2.5×) were used. Initially, dodecane was employed as the bulk organic phase, which does not evaporate appreciably over the time scale of these studies (see SI, Figure S-1). As outlined in the experimental section, this solution contained 0.35 M amorphous calcium carbonate (ACC) from the core of an overbased detergent and a droplet containing 0.5 M $H_2SO_4$.

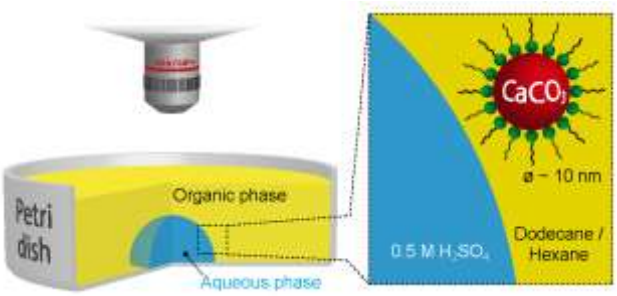


**Figure 1.** Schematic of experimental setup, representing a $H_2SO_4$ droplet surrounded by overbased calcium carbonate detergent particles in oil.

Due to the immiscibility of aqueous solutions with dodecane, a well-defined interface was established (see Figure 2a). Figure 2b shows a snapshot of the resulting crystal growth (after six hours) for the whole interface (for further images and a full video of this process, see Figure S-2a and 'video_dodecane_overall.avi' in the SI). The first crystals were detected after approximately three hours, nucleating at the aqueous-organic interface and initially, spreading mainly into the aqueous droplet. This modification evidently led to a decrease of surface tension, with the interface expanding outward and crystal growth progressing in the oil phase. To determine the morphology of these crystals, a higher magnification (20×) was employed to fully resolve crystal growth directly at the interface. This highlighted the presence of needle-shaped crystals (see Figure 2c and Figure S-2b and 'video_dodecane_interface.avi' in the SI). A representative crystal was imaged at 100× magnification and analyzed using interferometry. Figures 2d and 2e demonstrate that the crystal had a very smooth, featureless surface (on this scale), which was true for all other crystals analyzed throughout the sample (see SI, Figure S-3).

The hydrated phase of these needle-shaped crystals was determined using Raman spectroscopy. Due to the small spot size of the laser (515 nm radius; calculated from the laser wavelength and the numerical aperture of the lens),[33] it was possible to obtain Raman spectra

corresponding only to the crystal of interest. Figure 3a shows that the crystals analyzed gave a strong peak centered at 1008 $cm^{-1}$, which corresponds to the $\nu_1$ $SO_4$ shift for gypsum ($CaSO_4 \cdot 2H_2O$), which has been previously reported at 1008 – 1010 $cm^{-1}$.[20,34-36] Due to the higher degree of hydration in the crystal structure, this peak occurs at lower wavenumbers than for bassanite ($CaSO_4 \cdot 0.5H_2O$), present at 1015 – 1016 $cm^{-1}$,[20,35,36] and anhydrite ($CaSO_4$), at 1017 – 1018 $cm^{-1}$.[20,34-36] This is therefore a definitive way of deducing the calcium sulfate phase grown. To further confirm this finding, Figure 3b shows that all crystals analyzed had a peak at 3404 $cm^{-1}$, corresponding to the $\nu_1$ $H_2O$ shift of gypsum (previously reported at 3404 – 3407 $cm^{-1}$).[20,36] Again, this is proof that these crystals are the dihydrate phase, as the $\nu_1$ $H_2O$ peak occurs at higher wavenumbers for bassanite, at 3556 $cm^{-1}$,[20] and is absent for anhydrite. The absence of the $\nu_3$ $H_2O$ gypsum peak (at 3494-3500 $cm^{-1}$)[20,36] in both the reference and sample spectra is most likely due to variations in crystal orientation, or may also indicate the presence of impurities and irregularities within the crystal structure.[36]

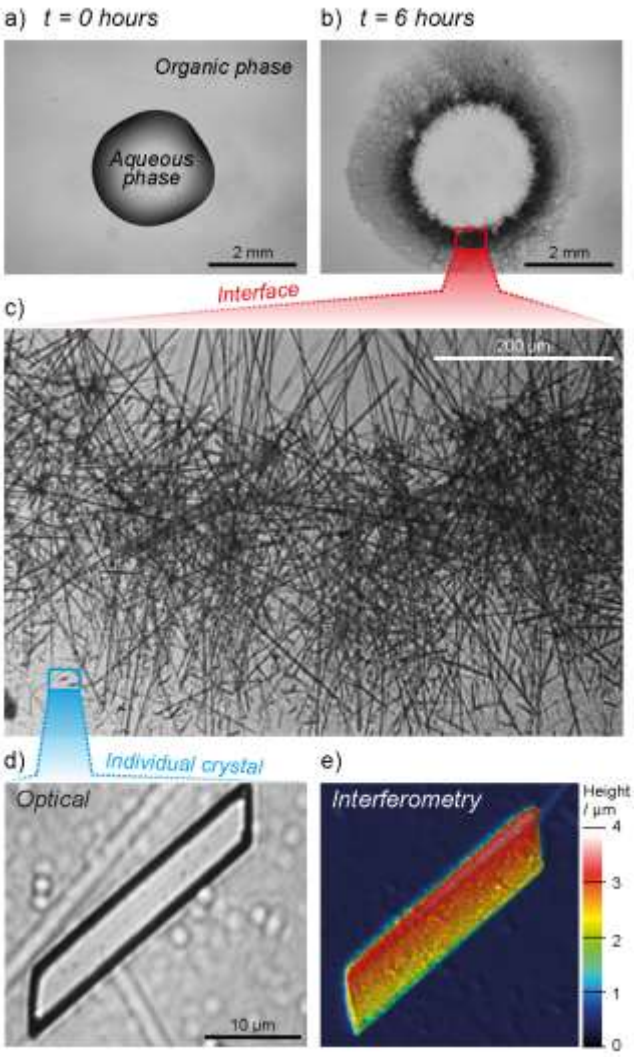


**Figure 2.** Results obtained for a configuration comprising 0.35 M $CaCO_3$ in 2 mL dodecane and a droplet containing 0.5 M $H_2SO_4$. a) Optical image of a 1 µL droplet in dodecane, b) optical image of overall crystal growth for a 1 µL droplet, c) optical image of crystal growth at the interface of a 20 µL droplet, d) optical image of a typical needle crystal formed during the experiment, and e) interferometry image of the same crystal.

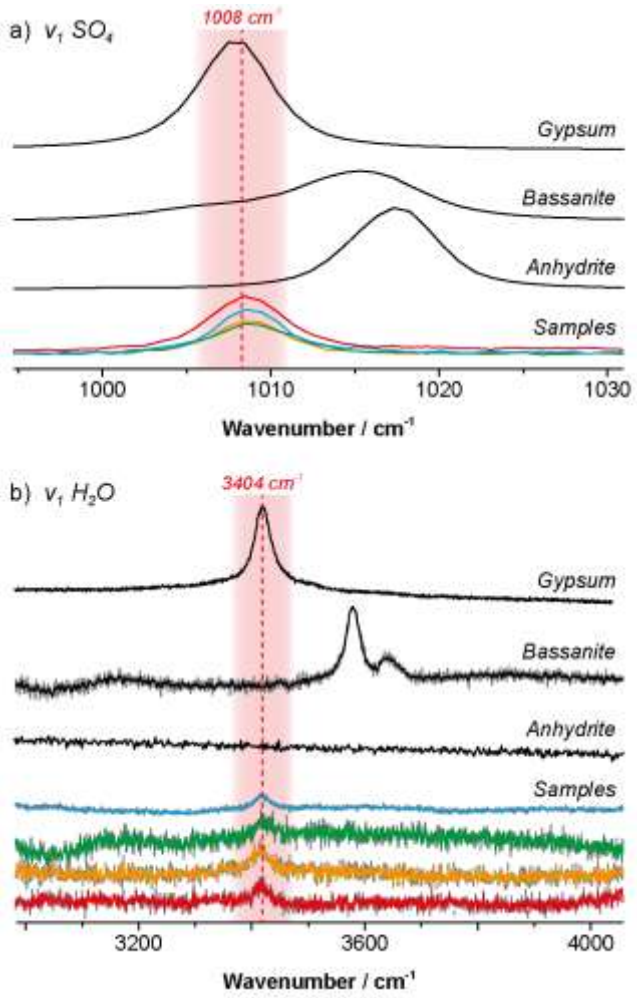


**Figure 3.** Raman reference spectra for gypsum, bassanite and anhydrite, together with spectra (bottom in each case) obtained for a range of samples grown in dodecane.

**Mechanism of the ACC-Gypsum Transition**

It is clear from these results that the initial ACC core of the overbased detergent in the oil phase reacts with $SO_4^{2-}$ ions from the aqueous droplet, to form the dihydrate phase of calcium sulfate, gypsum. It has been shown previously that when overbased calcium carbonate detergent particles are exposed to water, a thin film with a thickness of one or two water molecules forms between the ACC core and the stabilizing sulfonate head groups.[37] Thus, for the system employed in our work, it is plausible that the presence of the $H_2SO_4$ droplet results in the

formation of an aqueous $SO_4^{2-}$ layer, in direct contact with the ACC core. To test this idea, Karl Fischer measurements were conducted for pure hexane and dodecane solvents, as well as bulk solutions of hexane and dodecane containing 0.35 M $CaCO_3$ overbased detergent particles (the same concentrations and volumes as those used in crystal growth experiments). Table 1 shows that addition of the overbased detergent particles resulted in a similar increase in the water content of both solvents, implying that these particles already contain a small amount of water.

Although the sampling of these solvents was in bulk solution, we expect these results to be representative of the immiscible two-phase system used. Previous analysis of similar interfaces shows the bulk phase has a similar water content to the organic solvent close to the interface. For example, molecular dynamics calculations of the water-1,2-dichloroethane (DCE) interface show this is molecularly sharp, with no substantial region of strong mixing.[38] Neutron reflectivity measurements support this.[39] Synchrotron X-ray reflectivity measurements and predictions from capillary-wave theory give interfacial widths of the water-hexane and water-dodecane interfaces in the range of 3-5 Å.[40] This suggests that the interfaces employed in our crystal growth experiments will be very smooth.

**Table 1.** Karl Fischer water content values obtained for hexane and dodecane, in the presence and absence of 0.35 M $CaCO_3$ overbased detergent particles (error = ± 0.02 wt %).

| | **Water content values / wt %** | | | |
|---|---|---|---|---|
| | **Hexane** | | **Dodecane** | |
| | **Test 1** | **Test 2** | **Test 1** | **Test 2** |
| **Solvent only** | 0.00 | 0.00 | 0.00 | 0.00 |
| **$CaCO_3$ particles** | 0.13 | 0.13 | 0.10 | 0.14 |

Interestingly, the pseudomorphic replacement of calcite by an epitaxial layer of $CaSO_4$ (either gypsum, bassanite or anhydrite depending on the temperature of the reaction) has recently been reported.[20] This was achieved by part-dissolving millimeter-sized calcite pieces in $H_2SO_4$. At room temperature, gypsum was the precipitating phase, due to a closer match between the gypsum and calcite structures, compared to the other calcium sulfate hydrates. However, the formation of the gypsum layer passivates calcite and only a thin surface layer of gypsum is formed.[20] It is likely that an analogous mineral replacement reaction takes place in our system, but the process goes to completion because the parent phase in our system is in the form of nanoparticles, and a large percentage of the $CaCO_3$ is present at the nanoparticle surface and is thus highly accessible to the surrounding $SO_4^{2-}$-containing fluid. The hydrated $CaSO_4$ produced is the precursor to the gypsum that grows as needles in the aqueous phase and, ultimately, within the oil phase due to stabilization of the nanoparticles by the hydrophobic alkyl sulfonate surfactant.

**Crystal Growth Characteristics in the Aqueous-Hexane System**

Hexane is much more volatile than dodecane, and therefore evaporates if the system is left open to the atmosphere. This serves to gradually increase the calcium concentration during the course of a crystallization experiment in a similar way to other crystal growth strategies, such as the Kitano method, used to produce calcite.[41] The timescale of evaporation was that a negligible amount of organic solvent remained after 35 minutes (less than 0.5 wt. % - see SI, Figure S-1).

Crystal growth of the entire aqueous droplet interface was initially analyzed (see Figure 4a and Figure S-4a and 'video_hexane_overall.avi' in the SI). For the first 30 minutes, and in contrast to the dodecane case, the aqueous droplet appeared highly unstable, which was most likely a consequence of the evaporation of the hexane solvent causing convection. Crystal growth became apparent after approximately 30 minutes, when most of the hexane had evaporated resulting in a very high concentration of the calcium source.

To obtain a more in-depth understanding of the processes taking place, images were collected using a 20× objective lens (see Figure 4b and Figure S-4b and 'video_hexane_interface.avi' in the SI). As for the experiments performed in dodecane, although at the shorter times noted, needle growth initially occurred at the aqueous-organic interface, spreading both into and away from the droplet. These needles are likely to form via a similar mechanism as discussed above for dodecane, but in contrast, a higher density of needles formed in hexane, and these were about 10 times shorter than in the dodecane case. This can be rationalized: larger needles are likely to grow in dodecane, due to the presence of an inert solvent surrounding the aqueous droplet, which prevents evaporation and minimizes nucleation, in a similar way to the microbatch technique used to grow high quality protein crystals.[32]

A higher objective lens (100×) was used to determine the fate of the needles in the area of the glass surface highlighted in Figure 4b, which was previously covered with the bulk hexane

phase, prior to evaporation. Figure 4c shows snapshots of transitions apparent within this sample area (for further detail, see Figure S-4c and 'video_hexane_plates.avi' in the SI). After approximately two and a half hours, the needles produced began to reduce in length. Although the hexane solvent appeared to have fully evaporated by this stage of the experiment, the observation of needle dissolution suggests the presence of a thin interfacial fluid, an aspect that is discussed in more detail below.

After four hours, there was evidence of needles aligning parallel to each other (indicated by the arrows in the first image of Figure 4c and the red cross on the resulting crystal assembly). Examining the time shots in Figure 4c, precipitation of a new phase occurs, bridging the two parallel needles, which initially accumulates in the center (see crosses), and expands out along the length of the needles in both directions. This ultimately results in the formation of plate-shaped crystals, displaying a 'V' shape at each end (see second and third image of Figure 4c). Concurrently, small needles that did not transform into plates decrease in length and ultimately fully dissolve. Again, this dissolution would most reasonably be mediated by a thin interfacial fluid. At this time, very few needles surrounded the plate-like crystals. Over a period of 17 hours, the plate shaped crystals continue to grow, resulting in the 'V' shaped ends of some of these crystals transforming into 'rectangular' morphologies. This is evident in the final image of Figure 4c, taken after 21 hours. These transformations are rationalized later.

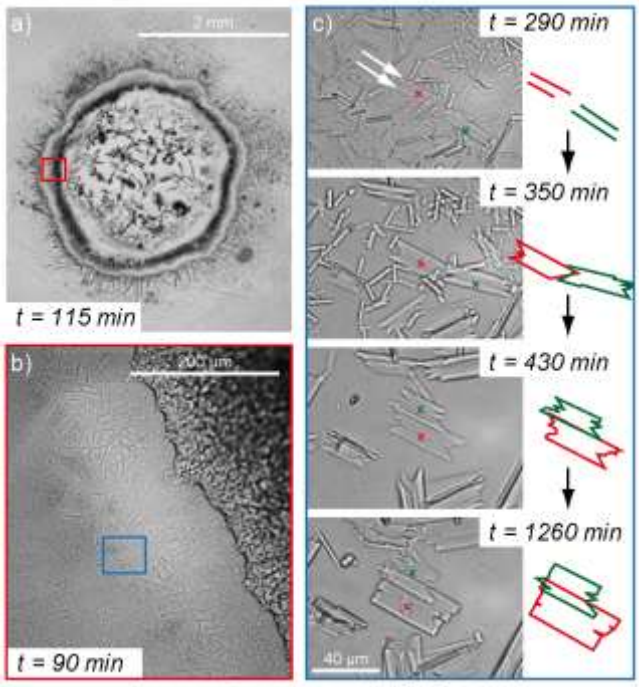


**Figure 4.** Optical images for a configuration comprising 0.35 M $CaCO_3$ in 2 mL hexane and an aqueous droplet containing 0.5 M $H_2SO_4$. a) Optical image of a 1 µL droplet in the hexane (organic) phase, showing crystal growth. b) Optical image of crystal growth near the interface of a 20 µL aqueous droplet. c) Optical images showing the transformation of needles to plates at various times.

Both interferometry and Raman spectroscopy were used to analyze the crystals in more detail, and to determine whether the different morphologies detected corresponded to different $CaSO_4$ hydrates. Figure 5 shows the three main crystal shapes selected, that are representative of the whole sample after all crystal growth had ceased and the hexane had fully evaporated (around eight hours). These include needles similar to those found in dodecane (crystal 1- Figure 5a), plates (crystal 3- Figure 5c) and crystals which appear to correspond to a stage between the two (crystal 2- Figure 5b). These were obtained from a range of sample areas, as shown in Figure S-5a in the SI (for further examples, see Figure S-5b in the SI). Needles were generally detected

near the position of the original aqueous droplet, whereas plates were detected further away from the droplet, in areas of the bulk organic phase, prior to evaporation. Crystals representing an intermediate stage were generally found between these two regions. Although plates were also detected in the center of the aqueous droplet (e.g. SI, Figure S-5), these formed over much longer periods (i.e. days rather than hours).

Interferometry measurements showed that the needles formed were relatively smooth, with very few surface features, as for crystallization with dodecane. In contrast, plates exhibited rougher surfaces. For crystals which represented an intermediate stage, there is evidence that these are comprised of individual needles that have come together, based on the overall crystal morphology (see Figure 5bi and bii). In addition, the 'V' shape previously seen in Figure 4c is also apparent in some of these intermediate states. The roughness profile in Figure 5bii shows a clear decrease in crystal height at the center of the 'V', with higher crystal edges, further confirming that growth is realized through the alignment of two parallel needles, which form the plate edges, with a progressive build-up of material between the two (for further roughness parameters, see SI, Figure S-5c).

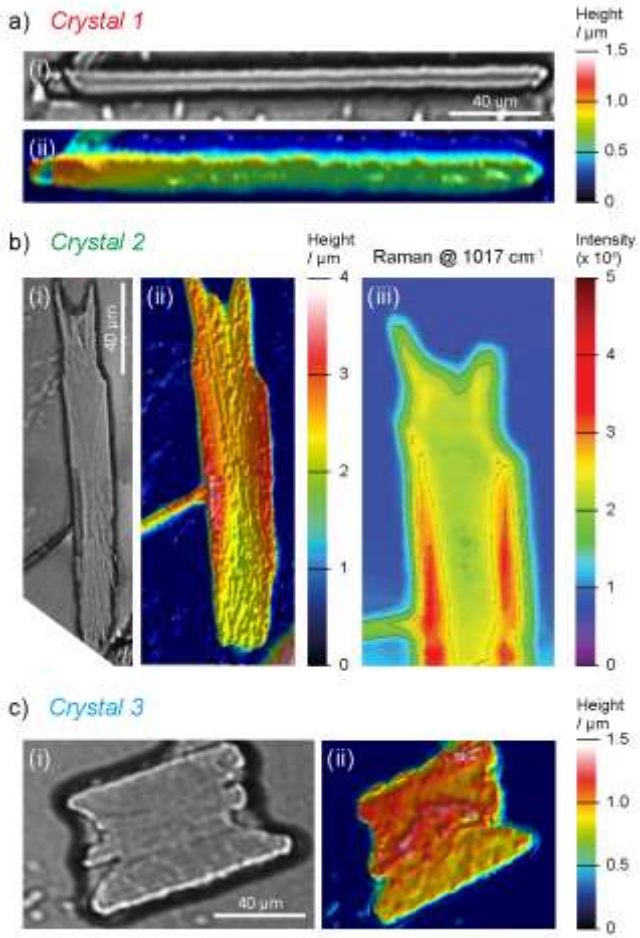


**Figure 5.** Micrographs of crystals from an experiment comprising 0.35 M $CaCO_3$ in 2 mL hexane and a 20 µL aqueous droplet containing 0.5 M $H_2SO_4$. ai) Optical and aii) interferometry images of crystal 1. bi) Optical and bii) interferometry images of crystal 2. biii) Raman map of crystal 2 acquired at 1017 $cm^{-1}$. ci) Optical and cii) interferometry images of crystal 3.

The Raman spectra in Figures 6a and b show that the needle-shaped crystal (crystal 1) gives rise to $\nu_1$ $SO_4$ and $\nu_1$ $H_2O$ shifts corresponding to gypsum. However, both the 'intermediate state' and plate crystals (crystals 2 and 3) give spectra that correspond to the fully dehydrated phase, anhydrite, displaying $\nu_1$ $SO_4$ shifts centered around 1017 $cm^{-1}$, and no peaks within the $\nu_1$

$H_2O$ region. Therefore, the needle-to-plate transition previously described corresponds to a gypsum-anhydrite transformation.

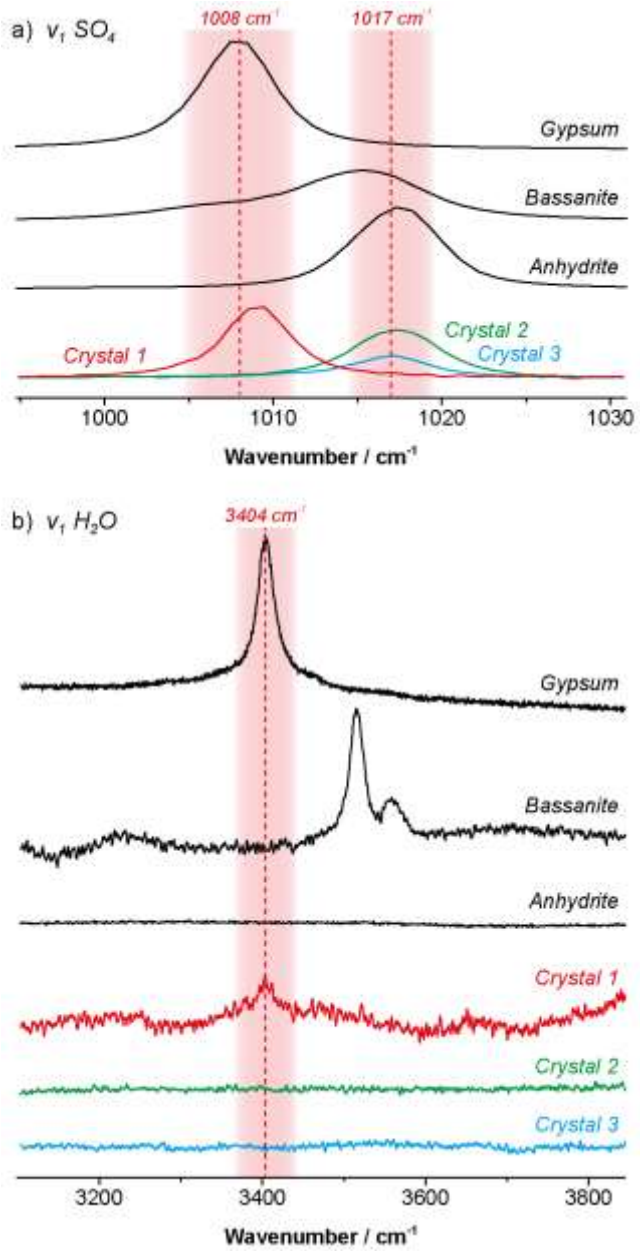


**Figure 6.** Raman reference spectra of gypsum, bassanite and anhydrite, together with spectra for crystals 1, 2 and 3 (samples) grown in hexane.

**X-ray Diffraction (XRD) Analysis**

To support the above analysis, powder X-ray diffraction (XRD) was performed, a technique used to determine the hydrated phase of all the crystalline material present in the whole sample. The results obtained are shown in Figure 7, and confirm all the crystals grown in dodecane correspond to gypsum, whereas both gypsum and anhydrite are present in the hexane sample. Furthermore, by comparing the crystallographic parameters for the anhydrite to reference data,[42] it is clear that this corresponds to insoluble anhydrite (see Table 2). For full crystallographic characterization of the gypsum and anhydrite polymorphs grown by the methodology, see Table S-6 in the SI.

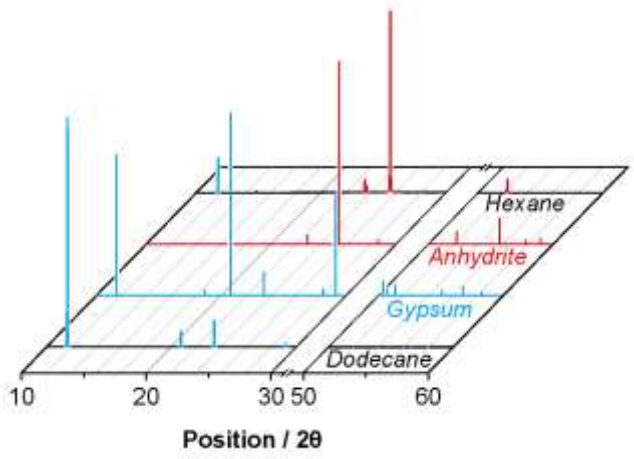


**Figure 7.** Powder XRD spectra for crystal samples produced in a system containing 0.35 M $CaCO_3$ in 2 mL hexane and dodecane and a 20 µL aqueous droplet containing 0.5 M $H_2SO_4$. Gypsum and anhydrite reference spectra are shown for comparison.

**Table 2.** Crystallographic parameters for the anhydrite grown, compared to reference data for soluble and insoluble anhydrite

| | Anhydrite data | Soluble anhydrite [a] | Insoluble anhydrite [a] |
|---|---|---|---|
| **Crystal system** | Orthorhombic | | |
| **Space group** | Cmcm | C222 | Amma |
| **Schönflies notation** | $\boldsymbol{D_{2h}^{17}}$ | $D_2^6$ | $\boldsymbol{D_{2h}^{17}}$ |
| **a / Å** | 6.993 | 6.972 | 6.998 |
| **b / Å** | 6.241 | 6.304 | 6.245 |
| **c / Å** | 7.002 | 12.078 | 7.006 |

[a] Data from reference 42 in the main text.

**Mechanism of the Gypsum-Anhydrite Transition**

Anhydrite plate growth was only achieved for experiments conducted in hexane, once the bulk organic phase had fully evaporated. In contrast, when non-volatile solvents such as dodecane were used, gypsum needles were the only crystalline phase grown. Indeed, when analogous experiments were conducted in hexane, but with the Petri dish sealed to prevent evaporation, only gypsum needles grew (see SI, Figures S-7 and S-8 and 'video_hexane_covered.avi'), confirming that organic solvent evaporation with concomitant increase in the concentration of the calcium detergent and enhanced mass transport drives this process. There is the possibility of either a solid-state transition in the absence of solvent, or a dissolution-precipitation mechanism within a thin interfacial fluid layer. We consider the latter to be more reasonable. As extremely small volumes of fluid are sufficient for dissolution-precipitation processes, solid-state transformations are not often realized.[16] It has been shown

that parts-per-million amounts of condensation water,[43] or even seven monolayers of water,[44] can induce this process. Both optical and interferometry images, as well as crystal growth videos, provide significant evidence for the dissolution of gypsum needles, shown through a decrease in length, as the dissolution flux is higher at the ends of each needle (see Figure 8a). This strongly indicates the presence of a thin interfacial layer, which must have some aqueous character, to allow the dissolution of this hydrated phase. This suggestion is reasonable given the existence of thin water films on surfaces subjected to atmospheric conditions, with thicknesses of approximately five monolayers of water.[45] Thus, the conditions in this thin interfacial film, which are largely different to those of bulk aqueous solutions, appear to aid gypsum dissolution and anhydrite precipitation. However, this thin interfacial layer is also likely to contain small residues of hexane solvent, and base oil from the detergent formulation, and thus would have a rather complex structure with a thickness greater than a few monolayers.

As the gypsum needles dissolve, $Ca^{2+}$ and $SO_4^{2-}$ ions are released into the thin aqueous film. $CaSO_4$ micelles are also likely to be within this film, formed from neutralization of the overbased $CaCO_3$ detergent particles by $H_2SO_4$,[46,47] and this component plays an important role. This was explored by studying the effects of adding hexane and/or detergent particles to a Petri dish containing gypsum seeds. The seeds were grown in the same way as for the dodecane crystal growth experiments, and each sample was rinsed with hexane to remove any excess detergent particles or surfactant. When only hexane was added to the gypsum seeds, no conversion to anhydrite was found at times as long as 48 hours. Similarly, when both hexane and detergent particles were added, no conversion was realized. The gypsum-anhydrite transition was only seen when the $H_2SO_4$ droplet was also present, suggesting the $CaCO_3$ cores of the overbased detergent must be converted to $CaSO_4$, providing a higher concentration of $CaSO_4$ material in the thin interfacial film.

Recent work demonstrates that by limiting the water content of a solution to 0.2 wt %, (resulting in a $CaSO_4$:$H_2O$ ratio of 1:0.5), it is possible for phase-pure anhydrite to precipitate at room temperature. This was achieved by dissolving equimolar amounts of $CaCl_2$ and $H_2SO_4$ in dry methanol.[8,11] Similarly, we suggest that in our system the high concentration of $CaSO_4$ within a very small volume of solvent would result in a thin interfacial fluid layer with a $CaSO_4$:$H_2O$ ratio sufficiently high to achieve the critical value for anhydrite precipitation. This idea is also supported by noting that the equilibrium constant for the conversion of gypsum to anhydrite is highly dependent on the temperature and solvent water activity.[15,18,26] Theoretically, if the water activity is lowered to values around 0.77, conversion can take place at temperatures as low as 23 °C.[26]

It is also important to point out that the structure of water in thin interfacial films exhibits very different properties to bulk water. It has been demonstrated that fully hydrogen-bonded, ice-like networks of water molecules form at the surface of amorphous $SiO_2$,[48] comparable to the glass surfaces used for crystal growth. The structural ordering in these thin interfacial films at the glass surface reduces the hydrogen-bonding ability of these water molecules in comparison to bulk water. This would inhibit the precipitation of the dihydrate $CaSO_4$ phase, gypsum, and favor the formation of the fully dehydrated phase, anhydrite.

Thus, the following are key features of the gypsum-anhydrite transition. When the gypsum needles are far away from each other, they dissolve until they completely disappear (see Figure 8b). However, if these needles align parallel to each other, there is diffusional overlap of the $Ca^{2+}$ and $SO_4^{2-}$ gradients from the dissolving crystals, leading to a supersaturated region, with respect to anhydrite, between the two needles, which is higher in the center (where the overlap is strongest), leading to anhydrite nucleation and growth (see Figure 8c). With time, the solid anhydrite material grows out towards the needle edges, forming the ‘V’ shapes seen (e.g. Figure

5), with further anhydrite growth causing the 'V' shaped ends to fill in, as shown in the optical images in Figure 4c. This transition is not realized in dodecane or covered hexane experiments, as the presence of highly hydrophobic solvents severely hinders gypsum dissolution. This has been confirmed in previous studies, where the use of non-polar solvents hinders the release of; (i) surface water from proteins;[32] and (ii) structural water molecules from gypsum, preventing transformation to the hemihydrate and fully dehydrated phases, bassanite and anhydrite.[11]

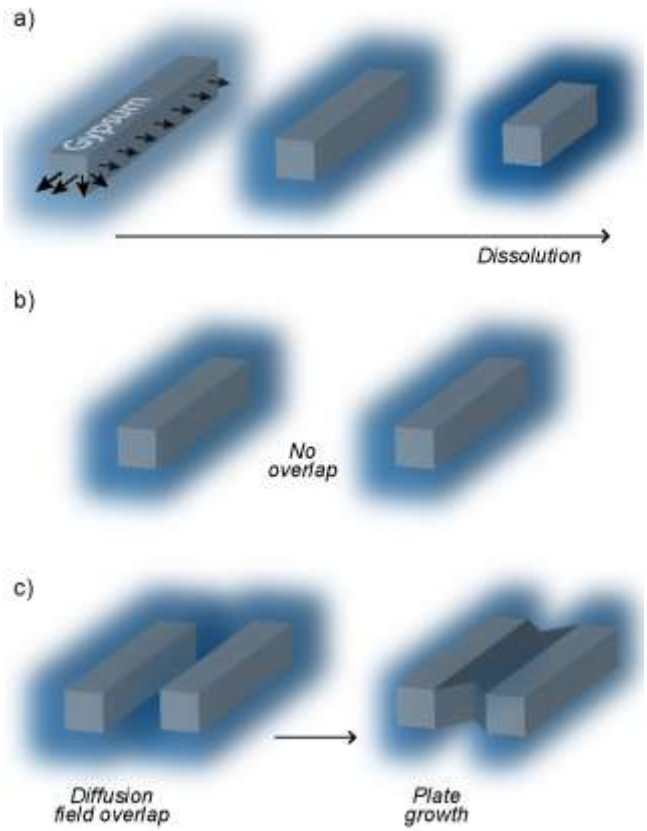


**Figure 8.** a) Schematic showing the directional fluxes of $Ca^{2+}$ and $SO_4^{2-}$ during the dissolution of the gypsum needles. b) Schematic showing that when two needles are separated, the diffusional fluxes do not interact significantly, but when in close proximity to each other as in c), the diffusional overlap results in the growth of plates with 'V' shaped ends.

We thus postulate that anhydrite crystal growth is achieved via a secondary nucleation mechanism, through conversion of initial gypsum needles. It is well known that primary anhydrite crystal growth is extremely difficult to achieve at moderate temperatures, due to the high kinetic barrier for its formation.[15,20,22,24,25,27] Therefore, secondary anhydrite nucleation via the formation of gypsum and/or anhydrite seeds is often realized,[17,18,26] and anhydrite crystallization has been witnessed to occur simultaneously with crystalline gypsum needle dissolution.[17] It is important to point out that, in our system, gypsum needles fully convert to anhydrite. For example, Raman maps for crystal 2 in Figure 5b, which exhibits the plate morphology with evidence of 'gypsum needle-like' side walls, confirmed that the whole crystal consisted of anhydrite only. This is evident from Figure 5biii which shows a map of the intensity of the $\nu_1$ $SO_4$ shift for anhydrite (at 1017 $cm^{-1}$), which has high intensity over the whole of the crystal shape. The stronger intensity of the anhydrite peaks at the crystal edges compared to the center is due to the crystal being higher in this region. This results in different anhydrite peak intensities across the crystal surface, correlating to the crystal height. A similar map was obtained at 1008 $cm^{-1}$ (the $\nu_1$ $SO_4$ shift for gypsum), showing no peaks, suggesting that all of the original gypsum needles have been fully converted to anhydrite. To support this, Raman spectra acquired at both the crystal edges and the center are shown in the Figure S-9 in the SI.

It has also been suggested that the excess free surfactant in overbased $CaCO_3$ detergent formulations is able to stabilize $H_2SO_4$ as microemulsion droplets, when used as an acid neutralization additive in internal combustion engines.[49] To examine whether the presence of free surfactant was important, experiments were also conducted using an overbased calcium carbonate detergent with a much higher free surfactant concentration. This detergent is stabilized by alkyl-phenate groups rather than sulfonate groups. For comparative analysis, a concentration was used that contained the same total base number as for the sulfonate detergent used in

experiments throughout this paper. The crystal growth characteristics were analogous to those seen for the sulfonate detergent, with growth of both gypsum and anhydrite occurring in hexane (see SI, Figure S-10 and 'video_phenate_overall.avi'). This suggests that the higher amount of free surfactant in the phenate detergent does not have a significant effect on the crystal growth process, and thus the free surfactant molecules do not play a significant role in controlling the gypsum-anhydrite transition.

Finally, it is worth considering whether gypsum directly converts to anhydrite, as suggested by the lack of bassanite detected from both Raman and XRD data, or whether bassanite is formed as a metastable phase, which may have been overlooked, as phase determinations were not carried out in situ. For aqueous systems, direct dehydration from gypsum to anhydrite is most often realized,[18,24,26] whereas for solid-state transitions occurring above 100 °C, stepwise dehydration is favored.[50-52] For solid-state transitions, the direct removal of all the water molecules from gypsum to form insoluble anhydrite would be unlikely, due to large differences in the two crystal structures. Likewise, the solid-state transformation of gypsum to the hemihydrate, bassanite, and then insoluble anhydrite, would also be difficult. This is because bassanite has a 'tunneled' crystal structure consisting of water channels, and further water removal to form insoluble anhydrite, with its close packed array structure with no channels would require a high amount of structural rearrangement.[50] This requires temperatures greater than 360 °C.[52] It is therefore extremely unlikely that this structure formed through solid-state transformations at room temperature, further reinforcing the dissolution-precipitation mechanism observed in our system.

## Conclusions

The transformation of gypsum to anhydrite has been successfully achieved at room temperature, using a two-phase aqueous-organic system. Using in situ microscopy and a range of structure-sensitive characterization techniques, we have been able to identify some of the key steps in the process. The new findings should be useful in constructing design rules to control crystallization and transformation in other crystal systems, for example, for calcium phosphates, which exhibit a variety of polymorphs that have various degrees of hydration.[15]

Our work has highlighted how simple, time-lapse light microscopy techniques can be used to identify important features of dissolution-precipitation mechanisms that lead to the transformation of gypsum to anhydrite, and that these features can then be confirmed through the application of a range of high-resolution microscopy and spectroscopic methods. The close alignment of gypsum microcrystals is an essential part of the process, with dissolution leading to favorable conditions to promote anhydrite crystallization in the region between the crystals. This highlights the significance of directional fluxes in crystallization and transformations that could be of importance in other systems.

## Associated Content

### Supporting Information

Videos of crystal growth, evaporation rates of organic solvents, further optical images of crystal growth, roughness parameters for crystals reported in the main paper, as well as additional examples, full characterization of crystallographic parameters for the crystals grown and optical images, Raman spectroscopy results for the covered hexane sample and calcium carbonate detergent with a high free surfactant concentration and additional Raman spectra from Raman maps (PDF). This material is available free of charge via the Internet at http://pubs.acs.org.

**Author Information**

**Corresponding Author**

* Email: P.R.Unwin@warwick.ac.uk

**Notes**

The authors declare no competing financial interest.

**Acknowledgements**

We acknowledge financial support from Lubrizol to E.R.R. We would like to thank Dr. David Walker for performing XRD experiments. We would also like to thank Lucy Broom for carrying out preliminary experiments prior to this work. The Panalytical XRD diffractometer used in this research was obtained through the Science City Advanced Materials Project: Creating and Characterizing Next Generation Advanced Materials, with support from Advantage West Midlands (AWM) and part funded by the European Regional Development Fund (ERDF).

**References**

(1) Mitchell, C. A.; Yu, L.; Ward, M. D. *J. Am. Chem. Soc.* **2001**, *123*, 10830-10839.

(2) Lang, M.; Grzesiak, A. L.; Matzger, A. J. *J. Am. Chem. Soc.* **2002**, *124*, 14834-14835.

(3) Hiremath, R.; Basile, J. A.; Varney, S. W.; Swift, J. A. *J. Am. Chem. Soc.* **2005**, *127*, 18321-18327.

(4) Belcher, A. M.; Wu, X. H.; Christensen, R. J.; Hansma, P. K.; Stucky, G. D.; Morse, D. E. *Nature* **1996**, *381*, 56-58.

(5) Naka, K.; Keum, D.-K.; Tanaka, Y.; Chujo, Y. *Chem. Commun.* **2000**, 1537-1538.

(6) Kotachi, A.; Miura, T.; Imai, H. *Cryst. Growth Des.* **2006**, *6*, 1636-1641.

(7) Xu, A.-W.; Dong, W.-F.; Antonietti, M.; Cölfen, H. *Adv. Funct. Mater.* **2008**, *18*, 1307-1313.

(8) Tritschler, U.; Van Driessche, A. E. S.; Kempter, A.; Kellermeier, M.; Cölfen, H. *Angew. Chem. Int. Ed.* **2015**, *54*, 4083-4086.

(9) Nielsen, M, H.; Li, D.; Zhang, H.; Aloni, S.; Han, T. Y.-H.; Frandsen, C.; Seto, J.; Banfield, J. F.; Cölfen, H.; De Yoreo, J. J. *Microsc. Microanal.* **2014**, *20*, 425-436.

(10) Chen, C.-L.; Qi, J.; Tao, J.; Zuckermann, R. N.; De Yoreo, J. J. *Sci. Rep* **2014**, *4*, 6222.

(11) Tritschler, U.; Kellermeier, M.; Debus, C.; Kempter, A.; Cölfen, H. *CrystEngComm* **2015**, *17*, 3772-3776.

(12) Herbstein, F. H. *Cryst. Growth. Des.* **2004**, *4*, 1419-1429.

(13) Bernstein, J. *Cryst. Growth. Des.* **2011**, *11*, 632-650.

(14) Seddon, K. R. *Cryst. Growth Des.* **2004**, *4*, 1087.

(15) Freyer, D.; Voigt, W. *Monatsh. Chem.* **2003**, *134*, 693-719.

(16) Ruiz-Agudo, E.; Putnis, C. V.; Putnis, A. *Chem. Geol.* **2014**, *383*, 132-146.

(17) Cody, R. D. F.; Hull, A. B. Method of growth of primary anhydrite crystals under moderate conditions. U.S. Patent 4,337,238, June 29, 1982.

(18) Azimi, G.; Papangelakis, V. G. *Hydrometallurgy* **2011**, *108*, 122-129.

(19) Wang, Y.-W.; Kim, Y.-Y.; Christenson, H. K; Meldrum, F. C. *Chem. Commun.* **2012**, *48*, 504-506.

(20) Ruiz-Agudo, E.; Putnis, C. V.; Hövelmann, J.; Álvarez-Lloret, P.; Ibáñez-Velasco, A.; Putnis, A. *Geochim. Cosmochim. Acta* **2015**, *156*, 75-93.

(21) Furby, E.; Glueckauf, E.; McDonald, L. A. *Desalination* **1968**, *4*, 264-276.

(22) Otálora, F.; Garcia-Ruiz, J. M. *Chem. Soc. Rev.* **2014**, *43*, 2013-2026.

(23) Serafeimidis, K.; Anagnostou, G. *Rock. Mech. Rock. Eng.* **2015**, *48*, 15-31.

(24) Fu, H.; Guan, B.; Jiang, G.; Yates, M. Z.; Wu, Z. *Cryst. Growth Des.* **2012**, *12*, 1388-1394.

(25) Ossorio, M.; Van Driessche, A. E. S.; Pérez, P.; García-Ruiz, J. M. *Chem. Geol.* **2014**, *386*, 16-21.

(26) Hardie, L. A. *Am. Mineral.* **1967**, *52*, 171-200.

(27) Ostroff, A. G. *Geochim. Cosmochim. Acta* **1964**, *28*, 1363-1372.

(28) Kashchiev, D. *Nucleation: Basic Theory with Applications*; Butterworth-Heinemann: Oxford, 1999.

(29) De Yoreo, J.J.; Velikov, P. G., Principles of crystal nucleation and growth. In *Reviews in Minerology and Geochemistry* in *Biomineralisation;* Dove, P. M., De Yoreo, J. J., Weiner, S., Eds.; Mineralogical Society of America: Virginia, 2003; Vol. 54, pp 57-93.

(30) Camacho D. M.; Roberts, K. J.; Lewtas, K.; More, I. *J. Cryst. Growth* **2015**, *416*, 47-56.

(31) Camacho Corzo, D. M.; Borissova, A.; Hammond, R. B.; Kashchiev, D.; Roberts, K. J.; Lewtas, K.; More, I. *CrystEngComm* **2014**, *16*, 974-991.

(32) Silver, B. R.; Fülop, V.; Unwin, P. R. *New J. Chem.* **2011**, *35*, 602-606.

(33) Renishaw, *inVia Raman microscope objective lens options*, Product note from the Spectroscopy Products Division, December 2006.

(34) Buzgar, N.; Buzatu, A.; Sanislav, I. V. *An. Stiint. U. Al. I-Mat* **2009**, *55*, 5-23.

(35) Liu, Y.; Wang. A.; Freeman, J. J. In *Raman, MIR, and NIR spectroscopic study of calcium sulfates: gypsum, bassanite, and anhydrite,* 40th Lunar and Planetary Science Conference, Houston, Texas, 2009.

(36) White, S. N. *Chem. Geol.* **2009**, *259*, 240-252.

(37) Tavacoli, J. W.; Dowding, P. J.; Steytler, D. C.; Barnes, D. J.; Routh A. F. *Langmuir* **2008**, *24*, 3807-3813.

(38) Benjamin, I. *J. Chem. Phys.* **1992**, *97*, 1432-1445.

(39) Strutwolf, J.; Barker, A. L.; Gonsalves, M.; Caruana, D. J.; Unwin, P. R.; Williams, D. E.; Webster, J. R. P. *J. Electroanal. Chem* **2000**, *483*, 163-173.

(40) Mitrinović, D. M.; Tikhonov, A. M.; Li, M.; Huang, Z.; Schlossman, M. L. *Phys. Rev. Lett.* **2000**, *85*, 582-585.

(41) Dobson, P. S.; Bindley, L. A.; Macpherson, J. V.; Unwin, P. R. *Langmuir* **2005**, *21*, 1255-1260.

(42) Christensen, A. N.; Olesen, M.; Cerenius, Y.; Jensen, T. R. *Chem. Mater*. **2008**, *20*, 2124-2132.

(43) Milke, R.; Neusser, G.; Kolzer, K.; Wunder, B. *Geology* **2013**, *41*, 247-250.

(44) Ruiz-Agudo, E.; Kudlacz, E.; Putnis, C. V.; Putnis, A.; Rodriguez-Navarro, C. *Environ. Sci. Technol.* **2013**, *47*, 11342-11349.

(45) Verdaguer, A.; Sacha, G. M.; Bluhm, H.; Salmeron, M. *Chem. Rev.* **2006**, *106*, 1478-1510.

(46) Wu, R. C.; Papadopoulos, K. D.; Campbell, C. B. *AIChE J.* **2000**, *46*, 1471-1477.

(47) Wu, R. C.; Papadopoulos, K. D.; Campbell, C. B. *AIChE J.* **1999**, *45*, 2011-2017.

(48) Asay, D. B.; Kim, S. H. *J. Phys. Chem. B.* **2005**, *109*, 16760-16763.

(49) Galsworthy, J.R.; Robinson, B. H., Glyde, R. W.; Hone, D. C., Colloidal Chemistry of Lubricating Oils. In *Reactions and Synthesis in Surfactant Systems;* Texter, J., Eds.; CRC Press: New York, 2001; Vol. 100, pp 387-388.

(50) Abriel, W.; Reisdorf, K. *J. Solid State Chem*. **1990**, *85*, 23-30.

(51) Hudson-Lamb, D. L.; Strydom, C. A.; Potgieter, J. H. *Thermochim. Acta* **1996**, *282-283*,

483-492.

(52) Prassad, P. S. R.; Pradhan, A.; Gowd, T. N. *Curr. Sci.* **2001**, *80*, 1203-1207.

**For Table of Contents Use Only**

Microscopic Studies of Calcium Sulfate Crystallization and Transformation at Aqueous-Organic Interfaces

*Emma R. Ravenhill,[1] Paul M. Kirkman,[2] and Patrick R. Unwin*[1]*

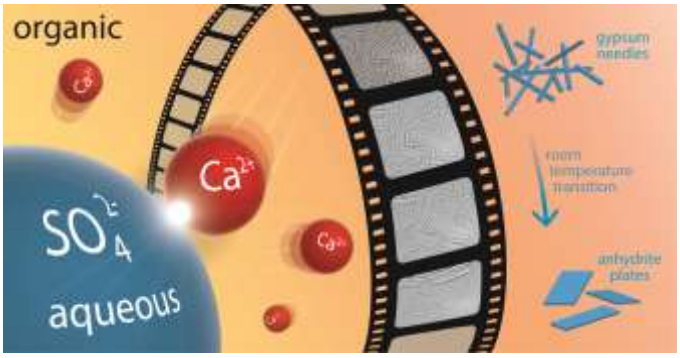


A novel approach has been developed for initiating calcium sulfate crystal growth at aqueous-organic interfaces. Synthesis of the most unstable form, anhydrite, rather than hydrated phases, can be achieved under ambient conditions, through a phase transition from gypsum needles.